 doi:10.20944/preprints201811.0459.v1

Effects of Sodium Substitution on the Rate Performances of Spherical $LiMn_2O_4$ Cathode for Lithium Ion Batteries

Jianbing Jiang[1,3],Wei Li, Haojie Deng and Lijian Xu[2,3,*]

[1]*College of Packaging and Material Engineering, Hunan University of Technology, Zhuzhou, 412007, China*

[2]*Hunan Key Laboratory of Biomedical Nanomaterials and Devices, College of Life Sciences and Chemistry, Hunan University of Technology, Zhuzhou 412007, P. R. China*

[3]*Foshan University, School of Materials Science and Energy Engineering, Foshan 528000, P. R. China*

* Correspondence: xljl235@hut.edu.cn; xlj235@163.com

Abstract

Sodium substitution $Li_{1-x}Na_xMn_2O_4$ cathodes were synthesized by a solid-state reaction method. The morphologies and crystal structures of $Li_{1-x}Na_xMn_2O_4$ were characterized by scanning electron microscopy (SEM) and X-ray diffraction (XRD), respectively. All $Li_{1-x}Na_xMn_2O_4$ samples exhibited a single phase $LiMn_2O_4$ spinel structure with good crystallinity. The effect of Na^+ ions on the electrochemical performance of $Li_{1-x}Na_xMn_2O_4$ was investigated by galvanostatic charge-discharge test. The results showed that lithium substituted by sodium deteriorated its capacity retention but enhance its discharge capacity when it worked at large current densities. The initial discharge capacity was 114.2 mAh/g for $Li_{0.94}Na_{0.06}Mn_2O_4$, and 93.1 mAh/g remained after 300 cycles at a current density of 2220 mA/g in the voltage range 3.0–4.3 V at room temperature.

Keywords: Lithium-Ion Battery, Cathode Material, Spinel $LiMn_2O_4$, Sodium, Substitution.

 doi:10.20944/preprints201811.0459.v1

1. INTRODUCTION

The serious energy crisis has promoted the research and development of chemical stored [1-3]. Lithium ion batteries provide four times the energy, half the weight, and longer life compared to lead acid battery systems. It makes a great contribution on small portable electronic devices, hybrid electric vehicles (HEV) and electric vehicles (EV) [4–8]. Among all the cathode materials, the spinel $LiMn_2O_4$ is considered as one of the most promising cathode materials for rechargeable LIBs due to its low cost, abundance, fast charge-discharge reactions, high coulombic efficiency and nontoxicity [9–14]. However, the large capacity loss of $LiMn_2O_4$ during the cycling process discourages further commercial use of the material. [15-18] The capacity fading during cycling is attributed to various factors, such as manganese dissolution in the electrolyte [19-21], Jahn–Teller distortion [22-25], and the formation of an oxygen deficiency [26]. To overcome these problems, many efforts have been devoted to modify the problems originating from the intrinsic characteristics of $LiMn_2O_4$. Cation doping is considered to be an effective strategy to alleviate the problems of $LiMn_2O_4$ by means of a series of transition metal substitution [21, 27-32].

$LiMn_2O_4$ is the cheapest lithium ion cathode, but its price is also many times that of lead acid battery, which limits its application in some fields. The high price of $LiMn_2O_4$ is mainly due to its raw materials. Electrolytic manganese dioxide (EMD) has been widely used as manganese compound precursors for synthesis of $LiMn_2O_4$ powders[33-35]. However, there is a mass of Na in EMD because alkali was adopted to neutralize during the progress of its progress. Li_2CO_3 prepared from salt lake or spodumene was

 doi:10.20944/preprints201811.0459.v1

another main material for producing $LiMn_2O_4$. However, there are also large amount of sodium in Li_2CO_3 because there are a mass of sodium in the salt lake. Many companies pay a lot of money to wash sodium in EMD or deal with sodium in salt lake, which results in the increasing price of $LiMn_2O_4$.

The effects of sodium substitution on the performances of $LiMn_2O_4$ must be studied in order to reduce its cost. In this work, a series of $Li_{1-x}Na_xMn_2O_4$ were prepared from Mn_3O_4, Li_2CO_3 and Na_2CO_3 by a solid state method. The effects of sodium substitution on the crystal structures, morphologies and electrochemical properties were investigated.

2. EXPERIMENTAL

2.1. Synthesis

Mn_3O_4 was prepared by controlled crystallization process with $MnSO_4$ and O_2 in water for about 12 h at 65-75℃. During the progress, ammonia solution was dropped to control the pH between 8.5 and 9.5. After the reaction was completed, the precipitate was filtered and washed by distilled water for three times and dried at 120C overnight. $Li_{1-x}Na_xMn_2O_4$ was prepared by a solid state synthesis from Li_2CO_3, Na_2CO_3 and the as-prepared Mn_3O_4.The mixture of Li_2CO_3, Na_2CO_3 and the as-prepared Mn_3O_4 (（Li+Na）/Mn = 1.03:2) was mixed with a mortar and pestle, then ground thoroughly and calcined at 650℃ for 8 h and 800℃ for 10 h in air. After cooling in furnace, the final black powder ($Li_{1-x}Na_xMn_2O_4$) was gotten.

2.2. Characterization

In order to identify the crystal structure, X-ray diffraction (XRD) analysis was

 doi:10.20944/preprints201811.0459.v1

performed using Philips X'Pert MPD (Philips) instrument with Cu Kα radiation. Scanning electronic microscopy (SEM) was performed using a JSM-5600LV (JEOL) instrument to detect surface morphology and analyze the size of the particles.

2.3. Electrochemical characterization

Electrochemical performance for the cathode was evaluated by assembling 2025-type coin cells with working cathode, lithium metal anode and celgard 2340 microporous membrane. The working cathode was fabricated using 80 wt% $Li_{1-x}Na_xMn_2O_4$ powders, 10 wt% carbon black and 10 wt% poly(vinyl difluoride) PVDF binder. 1M solution of $LiPF_6$ dissolved in ethylene carbonate (EC)/dimethyl carbonate (DMC) (1:1, in wt%) and obtained from Ferro Corporation was employed as electrolyte. The test cells were assembled into a glove box with an excellent environment control and the concentrations for both H_2O and O_2 were below 1 ppm. The charge–discharge performance for the cells was conducted on a battery test system (Land CT 2001A, Land Co. China). In the calculation of C-rate, 148 mA/g is assumed to be 1C. Electrochemical impedance spectroscopy (EIS) analysis were carried out under open circuit condition in the frequency range from 100 kHz to 0.005 Hz with 10 mV ac amplitude, conducted at CHI660D (CH Instruments).

3. RESULTS AND DISCUSSION

3.1. Morphology and Structure of Mn_3O_4

Fig.1 shows the SEM of the precursor prepared by the controlled crystallization method. It is obvious that Mn_3O_4 powders have helical spherical morphology in secondary

Preprints (www.preprints.org) | NOT PEER-REVIEWED | Posted: 19 November 2018 doi:10.20944/preprints201811.0459.v1

particles, while the primary particles are similar-sphere and they are densely agglomerated in secondary forms. This kind of morphology of helical spheres obviously comes from the formation of coordination compound of manganese ammoniate during the progress, which might plays a role in controlling not only the releasing velocity of manganese-ions, but also the growing direction of Mn_3O_4.

3.2. Morphology and Structure of $Li_{1-x}Na_xMn_2O_4$

The XRD patterns of $Li_{1-x}Na_xMn_2O_4$ are shown in Fig. 2. No obvious changes in the peak positions and intensities can be observed compared to the standard sample (JCPDS, card no. 35-0782). It indicated that the prepared $Li_{1-x}Na_xMn_2O_4$ samples possessed the cubic spinel structure with space group of Fd-3m, suggesting that the sodium substitution did not change the intrinsic cubic spinel structure, where Li^+ ions resided in the tetrahedral (8a) sites and Mn^{3+}/Mn^{4+} ions occupied the octahedral (16d) sites. The lattice constant was calculated according to the eight diffraction lines (as shown in Fig.2) by a Least Squares Method, and the results were shown in Fig.3. Because the ionic radius of Na^+ is bigger than that of Li^+, the lattice parameter increased linearly with the increase of sodium substitution content. The SEM images of all the synthesized $Li_{1-x}Na_xMn_2O_4$ powders were shown in Figure 4. As seen in Fig. 4, after firing, the sphere shape becomes more uniform and ordered. All the powder particles consisted of potato-shaped secondary particles. The first particle on the surface was changed from sphere to nanometer exfoliate after sodium substituted. It becomes more obvious when more sodium substituted lithium. However, some rod-like particles also appeared as the substitution of sodium increases more than 8%, which must be avoided because it will

Preprints (www.preprints.org) | NOT PEER-REVIEWED | Posted: 19 November 2018 doi:10.20944/preprints201811.0459.v1

impale the microporous membrane and result in the battery short circuit.

3.3. Electrochemical Properties

Fig. 5 shows the initial charge–discharge voltage profiles of sodium substituted $Li_{1-x}Na_xMn_2O_4$ at 0.1 C rate in the voltage range of 3.0-4.3V. For all samples, two well-defined potential plateaus can be observed, which correspond to that of a two-stage intercalation/de-intercalation process of lithium in spinel $LiMn_2O_4$. The detailed data of the charge-discharge capacity was summarized in Table 1. With the increase of sodium substitution, both of the initial charge and discharge specific capacity decreased. The decrease in capacities of sodium substituted electrodes may be due to the decrease in the concentration of Li^+. Therefore, further increase of sodium substitution is not preferred as it is detrimental to the high specific capacity.

Table 1 The detailed data of the initial galvanostatic charge-discharge capacity of $Li_{1-x}Na_xMn_2O_4$ (x=0-0.1).

Sample	$Li_{0.98}Na_{0.02}Mn_2O_4$	$Li_{0.96}Na_{0.04}Mn_2O_4$	$Li_{0.94}Na_{0.06}Mn_2O_4$	$Li_{0.92}Na_{0.08}Mn_2O_4$	$Li_{0.9}Na_{0.1}Mn_2O_4$
Charge capacity	134.1	132.6	130.1	123.6	121.1
Disharge capacity	126.5	125.2	124.7	120	117.2

Fig.6 compares the discharge capacity of $Li_{1-x}Na_xMn_2O_4$ electrodes at various current densities at room temperature, where the samples were cycled 5 times at each current density, and corresponding data are summarized in Table 2. As shown in Fig.6, the

Preprints (www.preprints.org) | NOT PEER-REVIEWED | Posted: 19 November 2018 doi:10.20944/preprints201811.0459.v1

discharge capacity decreases as the current density increases in all samples, but the discharge capacity decreases more slightly with increasing substitution ratio. This result confirms that the sodium substitution effectively enhances the rate capability.

Table 2 The detailed data of specific initial discharge capacity of $Li_{1-x}Na_xMn_2O_4$ (x=0-0.1) at various current densities at room temperature (values of the first cycle).

sample	Current density					
	14.8mA/g	74mA/g	148mA/g	740 mA/g	1480mA/g	2220mA/g
	Discharge capacity (mAh/g)	Discharge capacity (mAh/g)	Discharge capacity (mAh/g)	Discharge capacity (mAh/g)	Discharge capacity (mAh/g)	Discharge capacity (mAh/g)
$Li_{0.98}Na_{0.02}Mn_2O_4$	126.4	116.7	113.1	98.4	78.9	60.5
$Li_{0.96}Na_{0.04}Mn_2O_4$	125.3	118.6	114.3	107.6	84.9	72.8
$Li_{0.94}Na_{0.06}Mn_2O_4$	125.2	122.1	118.5	114.1	100.5	92.4
$Li_{0.92}Na_{0.08}Mn_2O_4$	120.1	117.5	114.7	110.6	101	92.7
$Li_{0.9}Na_{0.1}Mn_2O_4$	119.6	116.9	113.6	109.2	92.6	83.1

Cycle performance of $Li_{1-x}Na_xMn_2O_4$ samples was studied between 3.0 and 4.3V at room temperature at different specific current. The results that discharge at 2 C rate and 5 C rate were illustrated in Fig.7 and Fig.8, respectively. The corresponding data are summarized in Table 3. As shown in Fig.7, as the substitution of sodium increase from 2% to 10%, the initial discharge capacity of the cathode powders decrease slightly from 115.6mAh/g to 108.1mAh/g, but the capacity retention increased from 86.68% to 89.64%

Preprints (www.preprints.org) | NOT PEER-REVIEWED | Posted: 19 November 2018 doi:10.20944/preprints201811.0459.v1

after 100 cycles. It illustrates that sodium substitution enhances the performance of $LiMn_2O_4$ at low current density. However, the results were reversed when further increase the discharge current to 5 C rate. As shown in Fig.8, as the substitution content of sodium increase from 2% to 6%, the initial discharge capacity of the cathode powders increases from 94.5mAh/g to 114.2mAh/g, but the capacity retention decreases from 85.82% to 81.52% after 300 cycles. Thus, the sodium substitution may enhance the discharge capacity but decrease the cycle performance at large current density. There are two reasons for the high capacity of cathode substituted by sodium. The first reason is the formation of nanometer exfoliate particle (as shown in Fig.4) on the surface of cathode, which results in the short ion diffusion distance. The second reason is that the unit cell parameter (as shown in Fig.3) of $Li_{1-x}Na_xMn_2O_4$ was enlarged when lithium was substituted by sodium, lithium ion transference become easier which result in the high discharge capacity. However, the Jahn-teller become severer when the unit cell parameter becomes bigger, which result in the poor cycle performance of $Li_{1-x}Na_xMn_2O_4$ cathode.

Table 3. The detailed data of initial discharge capacity and capacity retention after 100 cycles of $Li_{1-x}Na_xMn_2O_4$ (x=0-0.1) (discharge at a constant specific current of 296mA/g at room temperature).

samples	Initials discharge capacity (mAh/g)	Discharge capacity after 100cycles (mAh/g)	Capacity retention (%)
$Li_{0.98}Na_{0.02}Mn_2O_4$	115.6	100.2	86.68%
$Li_{0.96}Na_{0.04}Mn_2O_4$	115.5	96.8	83.81%

Preprints (www.preprints.org) | NOT PEER-REVIEWED | Posted: 19 November 2018 doi:10.20944/preprints201811.0459.v1

$Li_{0.94}Na_{0.06}Mn_2O_4$	113.9	99.7	87.54%
$Li_{0.92}Na_{0.08}Mn_2O_4$	111.9	96.3	86.06%
$Li_{0.9}Na_{0.1}Mn_2O_4$	108.1	96.9	89.64

High temperature performance is an important parameter to estimate the electrochemical performance of a kind of electrode material. After comparing the results above, it can be found the rate capacity and cycle performance of $Li_{0.94}Na_{0.06}Mn_2O_4$ are very good. Thus, it was further study in the voltage range of 3.0-4.3 V at 55℃. Fig.9 shows the charge–discharge voltage profiles at various current densities. As the current density increases from 0.1 to 0.5, 1, 5, 10 and 15 C, the discharge capacity decreases slightly from 125.1 to 123.3, 119.6, 116.4, 102.3 and 93.2 mAh/g, respectively. Fig.10 shows the cycle performance curve at a constant specific current of 5C. The initial charge and discharge capacities are 114 mAh/g and 112.1 mAh/g, respectively. After 100 cycles, the charge and discharge capacities are 84.3 mAh/g and 82.9 mAh/g, the discharge capacity retention of $Li_{1.94}Na_{0.06}Mn_2O_4$ remains at 73.95%. Comparing with its cycle performance at room temperature, both the first discharge capacity and the discharge capacity retention decreased slightly. The poor cycle stability can be attributed to the dissolution of Mn ion at high temperature. Thus the cycle performance of sodium substituted $Li_{1-x}Na_xMn_2O_4$ must be improved by other ways, such as doping with other element or coating.

Electrochemical impedance spectroscopy analysis is an effective means to study the kinetics of the electrode reaction [36, 37]. In order to further elucidate the

Preprints (www.preprints.org) | NOT PEER-REVIEWED | Posted: 19 November 2018 doi:10.20944/preprints201811.0459.v1

electrochemical properties of the $Li_{1-x}Na_xMn_{2-x}O_4$ (x=0.02-0.1), EIS analysis of the composite electrodes at charged (4.3 V) state was been carried out. The measured impedance of the electrochemical cell is a collective response of the kinetic process occurring in the electrode. Fig.11 displays the electrochemical impedance spectra of $Li_{1-x}Na_xMn_{2-x}O_4$ electrodes. The equivalent circuit model and the resistance values obtained from fitting are given in the inset of the Fig.11. In the equivalent circuit, R_Ω is the ohmic resistance of the battery, including the total resistance of electrolyte, separator, conductive material, etc.; R_{ct} represents the charge transfer resistance; CPE (Constant phase element) is used to replace the capacitor in order to fit the experimental data appropriately; CPE1 corresponds to the surface film capacitance in high-frequency semicircle; and CPE2 corresponds to double layer capacitance in the low-frequency line. As can be seen in Fig.11, the charge transfer resistance of $Li_{1-x}Na_xMn_{2-x}O_4$ decreases from 424.7Ω to 227.9 with the increase of sodium substitution from 2% to 10%, confirming the role of sodium substation enabled high rate performance reported above.

4. CONCLUSION

The effects of sodium substitution on the performances of spherical $LiMn_2O_4$ cathode were studied in this paper. The sodium substitution does not change the basic spinel structure. But it affects the rate performance of $LiMn_2O_4$. Sodium substitution enhances its initial discharge capacity at large current density. As the molar ratio of sodium to lithium increase from 0.02 to 0.06, the initial discharge capacity increase from 94.5 to 114.2 mAh/g, and the capacity retention decreases from 85.82% to 81.52% after 300

 doi:10.20944/preprints201811.0459.v1

cycles at a current density of 740mA/g at room temperature.

Acknowledgements This work was supported by the National Natural Science Foundation of China (51604106), Foundation of Hunan Province Department of Education (16C0458), and the China Postdoctoral Science Foundation(2016M602428).

References and Notes

[1] Chen J. J.; Kwan A. K. H.; Jiang Y. Adding limestone fines as cement paste replacement to reduce water permeability and sorptivity of concrete. *Constr. Build Mater*. 2014, 56, 87-93.

[2] Zhou Y. L.; An J.; Luo D. M.; Hu W. Microstructures and mechanical properties of as cast Mg-Zr-Ca alloys for biomedical applications. *Mater. Technol.* 2012, 27, 52-54.

[3] Chen J. W.; Wang X. C.; Yu X. M. High dielectric constant and low dielectric loss poly (vinylidene fluoride) nanocomposites via a small. *J. Mater. Chem.* 2018, 6, 271-279.

[4]Cao Z.; Wei B. Fragmented carbon nanotube macrofilms as adhesive conductors for lithium-ion batteries. *ACS Nano.* 2014, 8, 3049–3059.

[5] Noh H. K.; Park H. S.; Jeong H. Y.; Lee S. U.; Song H. K. Doubling the capacity of lithium manganese oxide spinel by a flexible skinny graphitic layer. *Angew. Chem.* 2014, 53, 5059–5063.

[6] Martinez S.; Sobrados I.; Tonti D.; Amarilla J. M.; Sanz J. Chemical vs.

 doi:10.20944/preprints201811.0459.v1

electrochemical extraction of lithium from the Li-excess $Li_{1.10}Mn_{1.90}O_4$ spinel followed by NMR and DRX techniques. *Phys. Chem. Chem. phys.* 2014, 16, 3282–3291.

[7] Lee K. T.; Jeong S.; Cho J. Roles of surface chemistry on safety and electrochemistry in lithium ion batteries. *Accounts Chem. Res.* 2013, 46, 1161–1170.

[8] Jayaraman S.; Aravindan V.; Suresh K. P. Synthesis of porous LiMn2O4 hollow nanofibers by electrospinning with extraordinary lithium storage properties. *Chem. Commun.* 2013, 49, 6677-6679.

[9] Li N.; Wei W.; Xie K. Y. Suppressing dendritic lithium formation using porous media in lithium metal based batteries. *Nano. Letters*, 2018, 18, 2067–2073.

[10] Ragavendran K. R.; Xia H.; Yang G.; Vasudevan D.; Emmanuel B.; Sherwood D.; Arof A. K. On the theory of high rate capability of LiMn2O4 with some preferred orientations: insights from the crystal shape algorithm. *Phys. Chem. Chem.* Phys. 2014, 16, 2553–2560.

[11] Lee M. J.; Lee S.; Oh P.; Kim Y.; Cho J. High performance LiMn2O4 cathode materials grown with epitaxial layered nanostructure for Li-ion batteries. *Nano. Letters*, 2014, 14, 993–999.

[12] Sim C. M.; Choi S. H.; Kang Y. C. Superior electrochemical properties of $LiMn_2O_4$ yolk-shell powders prepared by a simple spray pyrolysis process. *Chem. Commun.* 2013, 49, 5973–5978.

[13] Bai M. H.; Xie K. Y.; Yuan K. A scalable approach to dendrite-free lithium anodes

via spontaneous reduction of spray-coated graphene oxide layers. *Adv. Mater.* 2018, 9, 1-7.

[14] Luo X. D.; Yin Y. Z.; Yuan M. High performance composites of spinel LiMn2O4/3DG for lithium ion batteries. *Rsc. Adv.* 2018, 8, 877-884.

[15]Hariprasada K.; Naresha N.; Raoc B.N.; Venkateswarlub M.; Satyanarayanaa N. Preparation of $LiMn_2O_4$ Nanorods and Nanoparticles for Lithium-ion Battery Applications. *Mater. Today,* 2016, 3, 4040-4045.

[16]Tron A.; Park Y. D.; Mun J. AlF_3-coated $LiMn_2O_4$ as cathode material for aqueous rechargeable lithium battery with improved cycling stability. *J. Power Sources,* 2016, 325, 360-364.

[17] Nageswara R. B.; Narsimulu D.; Srinadhu E. S. Structural, electrical, and dielectric properties of nickel-doped spinel $LiMn_2O_4$ nanorod. *Ionics*, 2018, 1-10.

[18] Douafer S.; Lahmar H.; Benamira M. Physical and photoelectrochemical properties of the spinel $LiMn_2O_4$, and its application in photocatalysis. *J. Phys. Chem. Solids,* 2018, 118, 62-67.

[19]Thackeray M. M.; Johnson C. S.; Kim J. S.; Lauzze K. C.; Vaughey J. T.; Dietz N.; Abraham D.; Hackney S. A.; Zeltner W.; Anderson M. A. ZrO_2- and Li_2ZrO_3-stabilized spinel and layered electrodes for lithium batteries. *Electrochem. Commun.* 2003, 5, 752-758.

[20]Tu J.; Zhao X. B.; Xie J.; Cao G. S.; Zhuang D. G. Zhu T. J.; Tu J. P. Enhanced low voltage cycling stability of $LiMn_2O_4$ cathode by ZnO coating for lithium ion batteries. J. *Alloys Compd.* 2007, 432, 313-317.

 doi:10.20944/preprints201811.0459.v1

[21]Arumugam D.; Kalaignan G. P. Synthesis and electrochemical characterization of nano-CeO_2-coated nanostructure $LiMn_2O_4$ cathode materials for rechargeable lithium batteries. *Electochim. Acta.* 2010, 55, 8709-8716.

[22]Li X. F.; Xu Y.; Wang C. Suppression of Jahn–Teller distortion of spinel $LiMn_2O_4$ cathode. *J. Alloys Compd.* 2009, 479, 310-313.

[23]Nakayama M.; Nogami M. A first-principles study on phase transition induced by charge ordering of Mn^{3+}/Mn^{4+} in spinel $LiMn_2O_4$ *Solid State Commun.* 2010, 150, 1329-1333.

[24]Rodrígueza R. A.; Pérez-Cappea E. L.; Laffitaa Y. M.; Ardanzab A. C.; Salazarc J. S.; Santosd M. Á.; Frutisd M. A.; Mohaleme N. D. S.; Alvesf O. L. Structural defects in $LiMn_2O_4$ induced by gamma radiation and its influence on the Jahn-Teller effect. *Solid State Ionics,* 2018, 324, 77-86.

[25]Liu W. W.; Wang. D.; Wang Z. Influence of magnetic ordering and Jahn-Teller distortion on the lithiation process of $LiMn_2O_4$. *Phys. Chem. Chem. Phys.* 2017, 19, 6481-6494.

[26]Komaba S.; Ogata A.; Shimizu T.; Ikemoto S. High temperature X-ray diffractive study of spinel-type lithium manganese oxides. *Solid State Ionics* 2008, 179, 1783-1787.

[27]Zhang L.; Lv X.; Wen Y.; Wang F.; Su H. Carbon combustion synthesis of $LiNi_{0.5}Mn_{1.5}O_4$ and its use as a cathode material for lithium ion batteries. *J. Alloys Compd.* 2009, 480, 802-805.

[28]Liu G. Q.; Wen L.; Liu G. Y.; Tian Y. W. Rate capability of spinel

 doi:10.20944/preprints201811.0459.v1

$LiCr_{0.1}Ni_{0.4}Mn_{1.5}O_4$. *J. Alloys Compd.* 2010, 501,233-235.

[29]Yang T.; Sun K.; Lei Z.; Zhang N.; Lang Y. J. The influence of holding time on the performance of $LiNi_{0.5}Mn_{1.5}O_4$ cathode for lithiums ion battery. *Alloys Compd.* 2010, 502, 215-219.

[30]Chen M. M.; Wu R. Y.; Ju S. G.; Zhang X. X.; Xue F.; Xing W. H. Improved performance of Al-doped $LiMn_2O_4$ ion-sieves for Li^+ adsorption. *Micropor. Mesopor. Mat.* 2018, 261, 29-34.

[31]Chung K. Y.; Yoon W. S.; Lee H. S. Comparative studies between oxygen-deficient $LiMn_2O_4$ and Al-doped $LiMn_2O_4$. *J. Power Sources*, 2005, 146, 226-231.

[32] Piao J. Y.; Duan S. Y.; Lin X. J. Surface Zn doped LiMn2O4 for an improved high temperature performance. *Chem. Commun.* 2018, 54, 5326-5329.

[33]Zhao Y. Q.; Jiang Q. L.; Wang W. G.; Du K.; Hu G. R. Effect of electrolytic MnO_2 pretreatment on performance of as-prepared $LiMn_2O_4$. *T. Nonferr. Metal. Soc.* 2012, 22, 1146-1150.

[34]Li B.; Wei X.; Chang Z. Facile fabrication of $LiMn_2O_4$, microspheres from multi-shell MnO_2, for high-performance lithium-ion batteries. *Mater. Lett.* 2014, 135, 75-78.

[35]Liu D.; Du L.; Liu Y. Effects of Mn-Precursor on Performances of $LiMn_2O_4$, Cathode Material for Lithium Ion Battery. *Rare. Metal. Mat. Eng.* 2014, 43, 2584-2587.

[36] Zhou Y. L.; Luo D. M. Microstructures and mechanical properties of Ti-Mo alloys cold-rolled and heat treated. *Mater. Charact.* 2011, 62, 931-937.

 doi:10.20944/preprints201811.0459.v1

[37] Nie B. H.; Zhao Z. H.; Liu S.; Chen D. C.; Ouyang Y. Z. Very High Cycle Fatigue Behavior of a Directionally Solidified Ni-Base Superalloy DZ4. *Mater.* 2018, 11, 98-109.

 doi:10.20944/preprints201811.0459.v1

Captions

Fig.1. SEM images of Mn_3O_4.

Fig.2. XRD patterns of $Li_{1-x}Na_xMn_2O_4$ (x=0-0.1).

Fig.3. Comparison plots of unit-cell parameters of $Li_{1-x}Na_xMn_2O_4$ (x=0-0.1) samples.

Fig. 4. SEM images of $Li_{1-x}Na_xMn_2O_4$ (x=0-0.1).

Fig.5 Initial galvanostatic charge–discharge curves of $Li_{1-x}Na_xMn_2O_4$ (x=0-0.1) between 3.0 and 4.3V at a constant specific current of 14.8mA/g.

Fig.6. Cycle performances of sodium substituted $Li_{1-x}Na_xMn_2O_4$ (x=0-0.1) at various rate capabilities in the potential range of 3.0–4.3 V at room temperature.

Fig.7. Cycle performance of $Li_{1-x}Na_xMn_2O_4$ (x=0-0.1) between 3.0 and 4.3V at a constant specific current of 296mA/g at room temperature.

Fig.8. Cycle performance of $Li_{1-x}Na_xMn_2O_4$ (x=0-0.1) between 3.0 and 4.3V at a constant specific current of 740mA/g at room temperature.

Fig.9. Charge–discharge curves of $Li_{0.94}Na_{0.06}Mn_2O_4$ at various rate capabilities in the potential range of 3.0–4.3 V at 55℃

Fig.10 Cycle performance of $Li_{0.94}Na_{0.06}Mn_2O_4$ at a constant specific current of 740mA/g in the potential range of 3.0–4.3 V at 55℃

Fig.11 Electrochemical impedance spectra for $Li_{1-x}Na_xMn_{2-x}O_4$ (x=0-0.1).

Preprints (www.preprints.org) | NOT PEER-REVIEWED | Posted: 19 November 2018 doi:10.20944/preprints201811.0459.v1

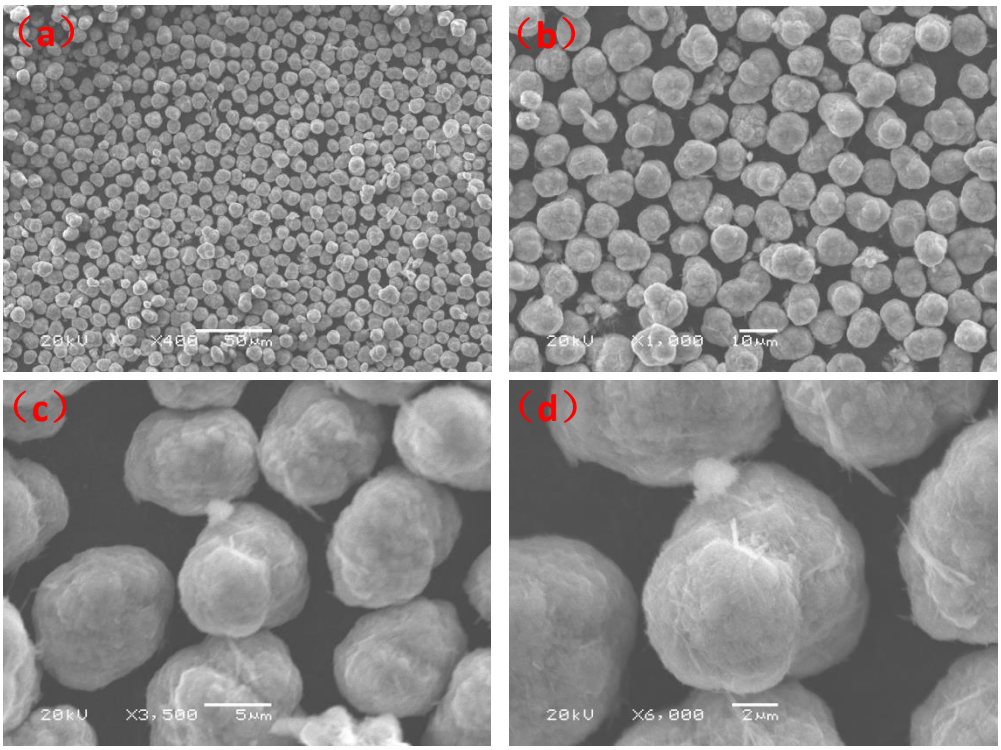

Fig.1. SEM images of Mn_3O_4 (a:×400， b:×1000， c:×3500， d:×6000)

Preprints (www.preprints.org) | NOT PEER-REVIEWED | Posted: 19 November 2018 doi:10.20944/preprints201811.0459.v1

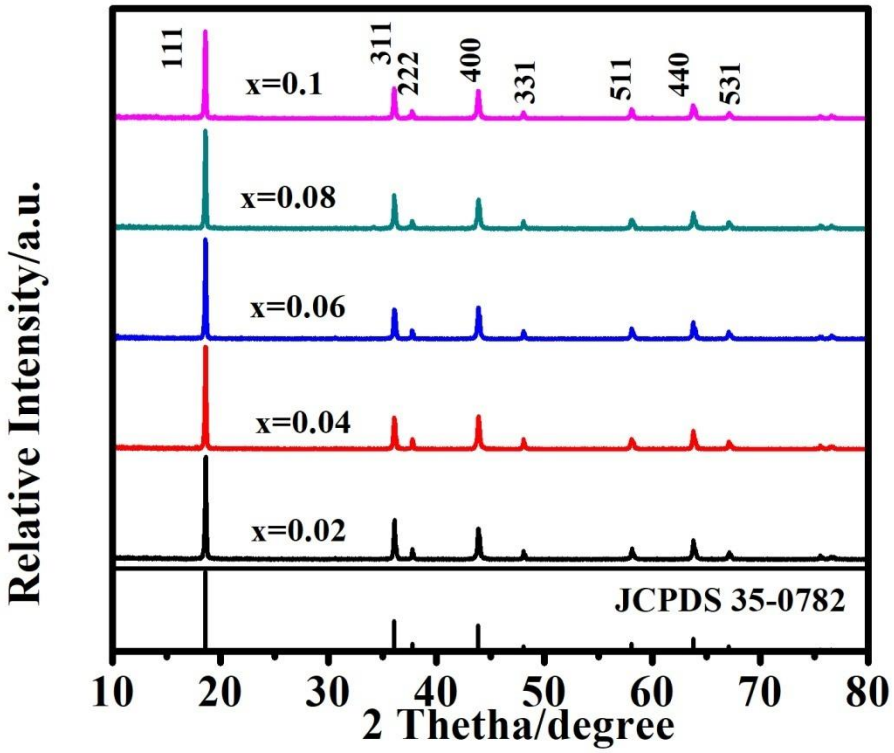

Fig.2. XRD patterns of $Li_{1-x}Na_xMn_2O_4$ (x=0-0.1).

Preprints (www.preprints.org) | NOT PEER-REVIEWED | Posted: 19 November 2018 doi:10.20944/preprints201811.0459.v1

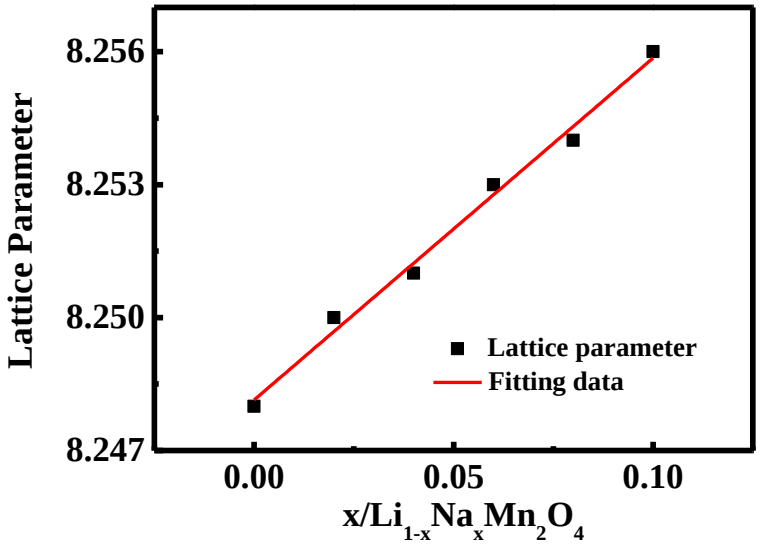

Fig.3. Comparison plots of unit-cell parameters of $Li_{1-x}Na_xMn_2O_4$ (x=0-0.1) samples.

Preprints (www.preprints.org) | NOT PEER-REVIEWED | Posted: 19 November 2018 doi:10.20944/preprints201811.0459.v1

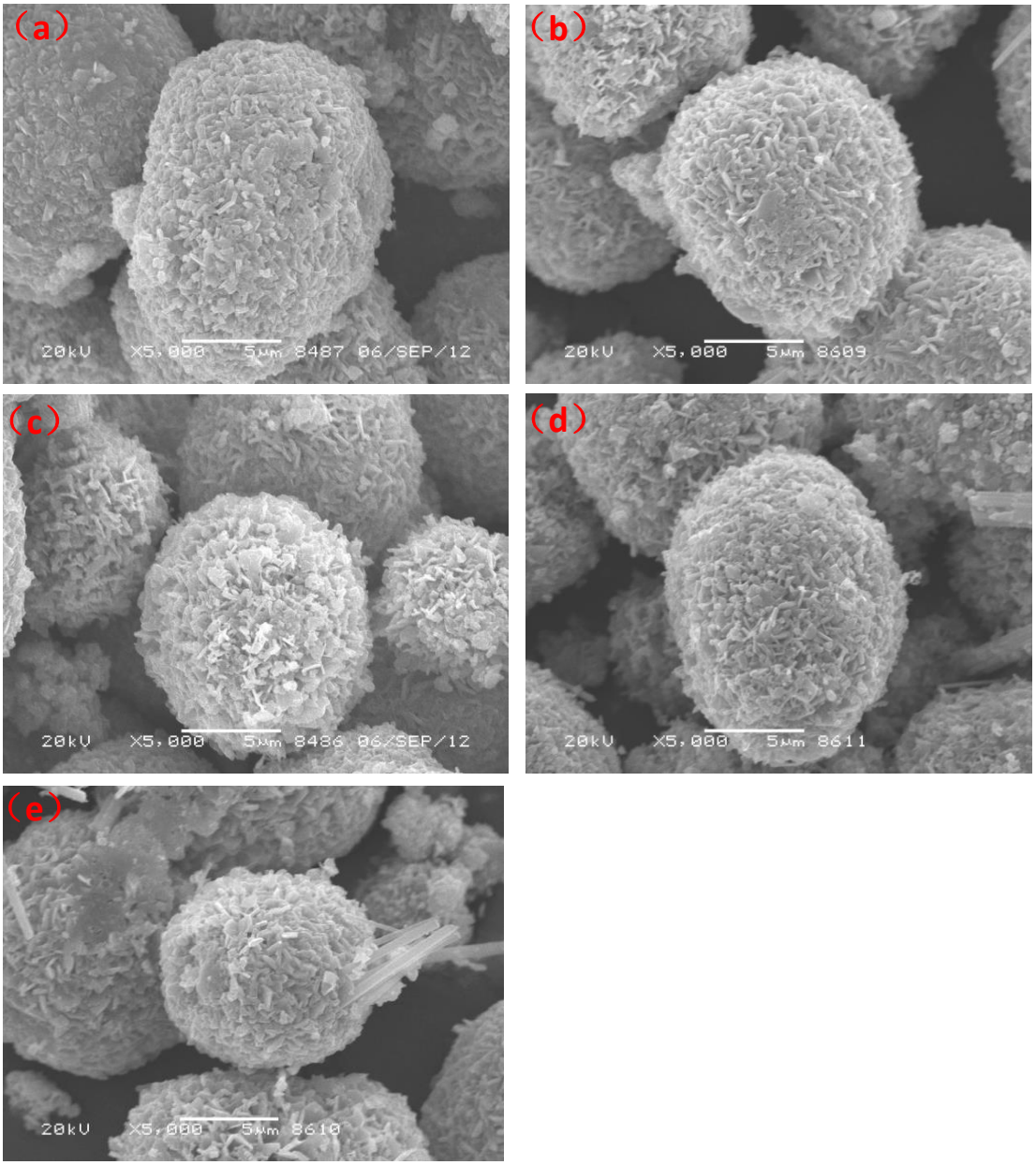

Fig. 4 SEM images of $Li_{1-x}Na_xMn_2O_4$ (x=0-0.1)： （a: $Li_{0.98}Na_{0.02}Mn_2O_4$； b： $Li_{0.96}Na_{0.04}Mn_2O_4$； c： $Li_{0.94}Na_{0.06}Mn_2O_4$； d： $Li_{0.92}Na_{0.08}Mn_2O_4$； b： $Li_{0.9}Na_{0.1}Mn_2O_4$）.

Preprints (www.preprints.org) | NOT PEER-REVIEWED | Posted: 19 November 2018 doi:10.20944/preprints201811.0459.v1

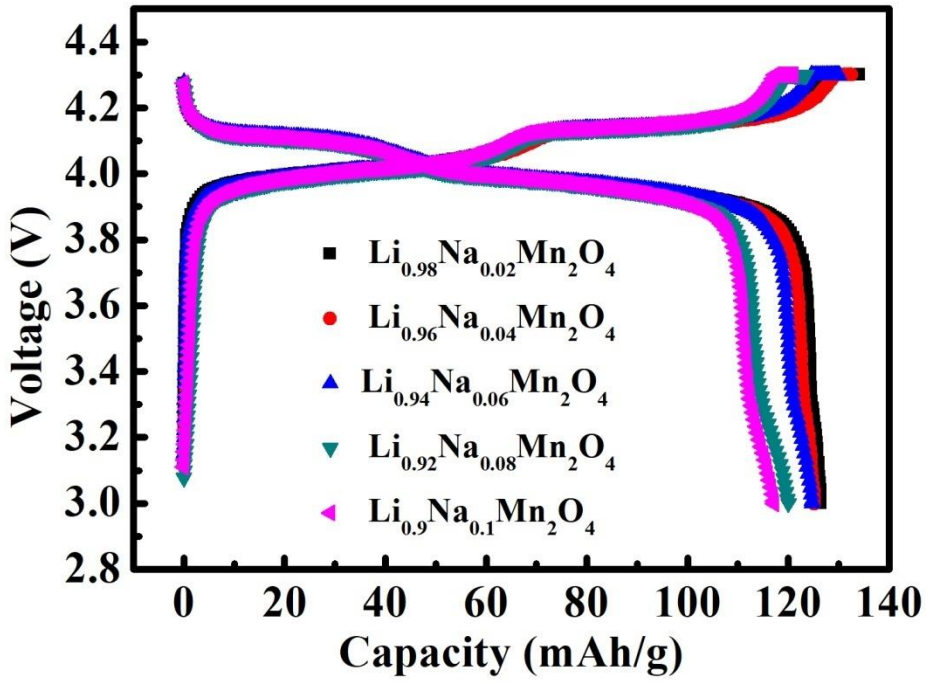

Fig.5 Initial galvanostatic charge–discharge curves of $Li_{1-x}Na_xMn_2O_4$ (x=0-0.1) between 3.0 and 4.3V at a constant specific current of 14.8mA/g.

Preprints (www.preprints.org) | NOT PEER-REVIEWED | Posted: 19 November 2018 doi:10.20944/preprints201811.0459.v1

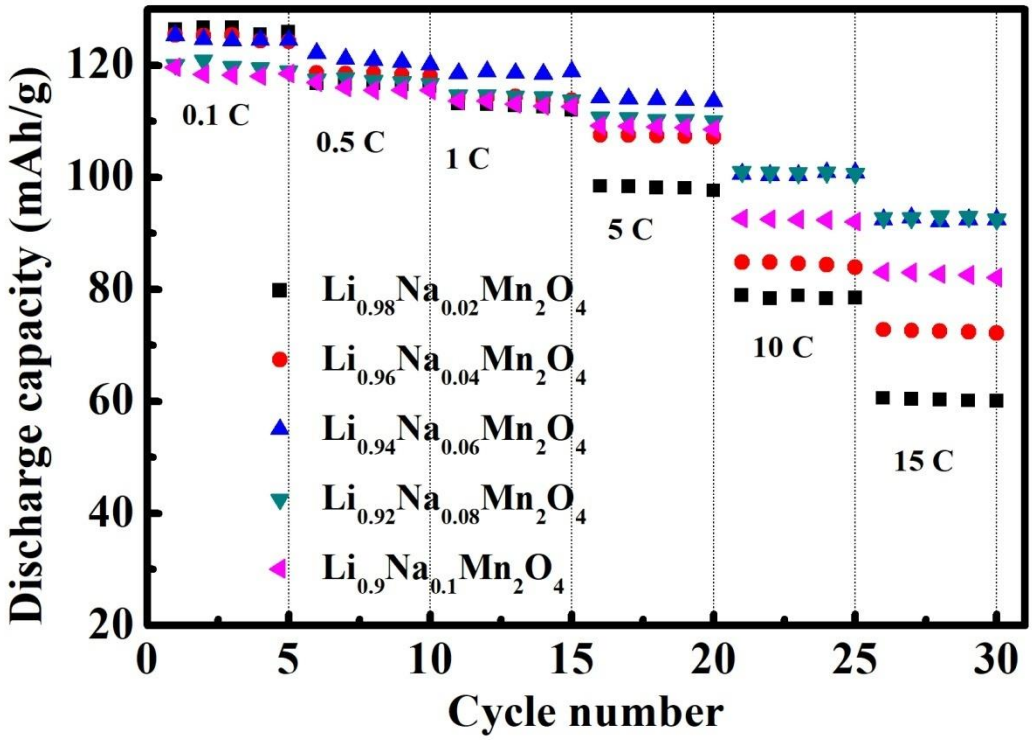

Fig. 6 Cycle performances of sodium substituted $Li_{1-x}Na_xMn_2O_4$ (x=0-0.1) at various rate capabilities in the potential range of 3.0–4.3 V at room temperature.

Preprints (www.preprints.org) | NOT PEER-REVIEWED | Posted: 19 November 2018 doi:10.20944/preprints201811.0459.v1

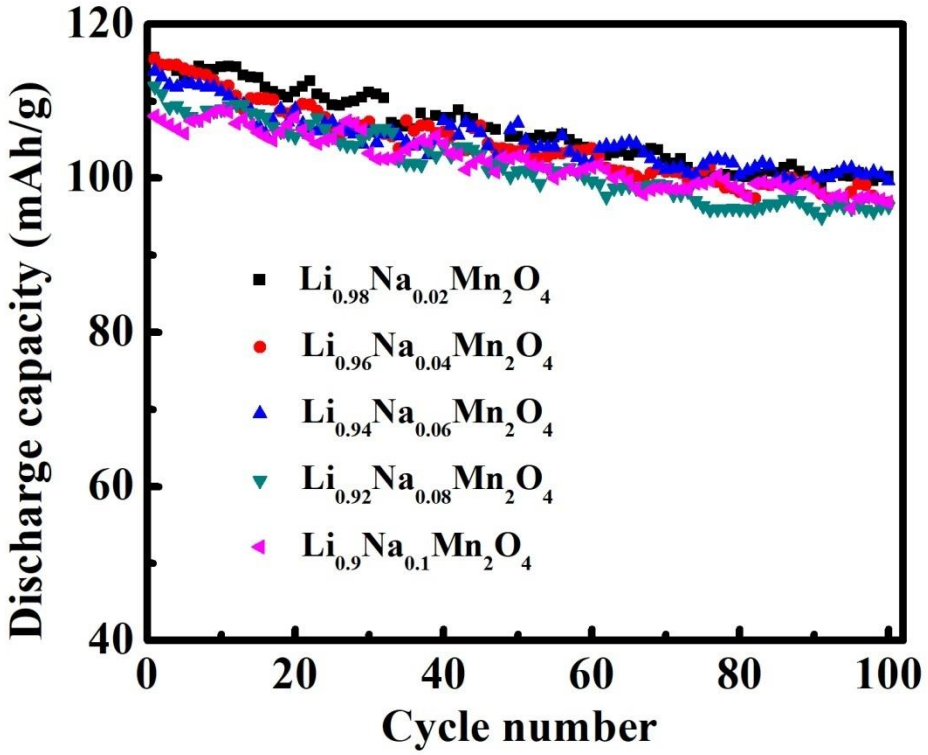

Fig.7 Cycle performance of $Li_{1-x}Na_xMn_2O_4$ (x=0-0.1) between 3.0 and 4.3V at a constant specific current of 296mA/g at room temperature.

Preprints (www.preprints.org) | NOT PEER-REVIEWED | Posted: 19 November 2018 doi:10.20944/preprints201811.0459.v1

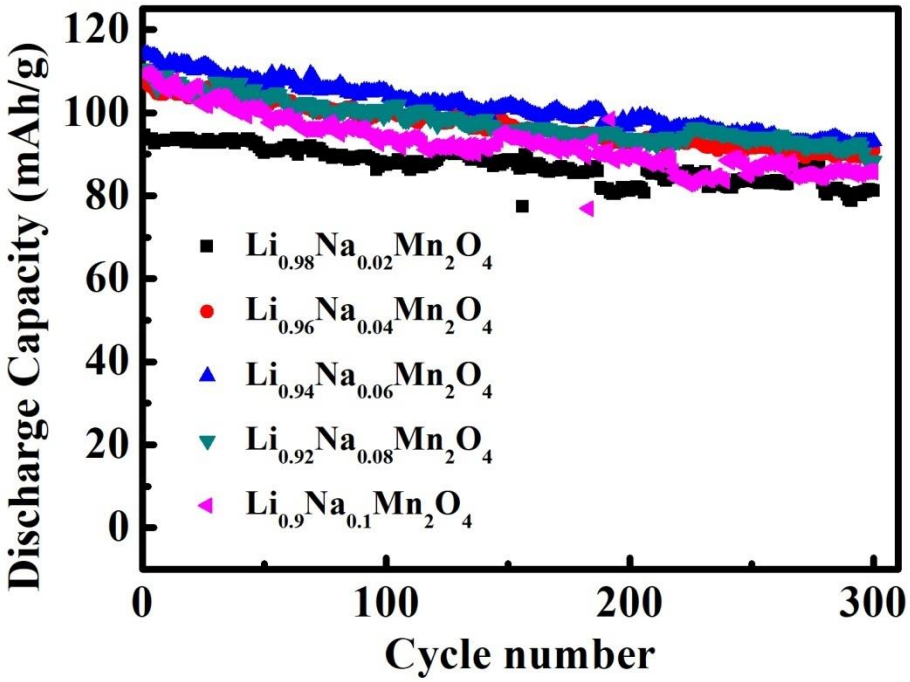

Fig.8 cycle performance of $Li_{1-x}Na_xMn_2O_4$ (x=0-0.1) between 3.0 and 4.3V at a constant specific current of 740mA/g at room temperature.

Preprints (www.preprints.org) | NOT PEER-REVIEWED | Posted: 19 November 2018 doi:10.20944/preprints201811.0459.v1

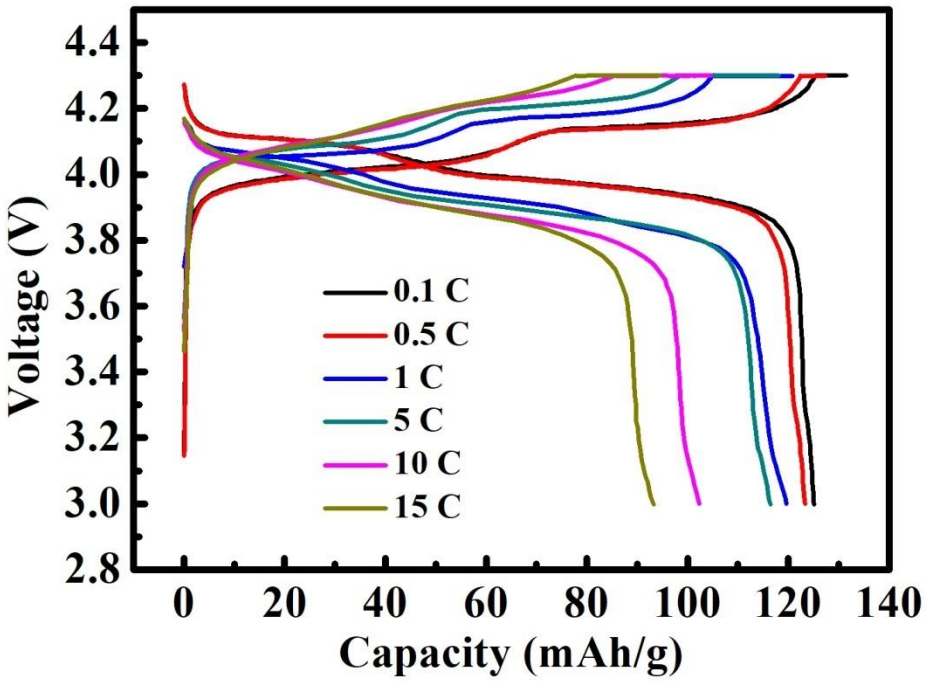

Fig.9 Charge–discharge curves of $Li_{0.94}Na_{0.06}Mn_2O_4$ at various rate capabilities in the potential range of 3.0–4.3 V at 55℃.

Preprints (www.preprints.org) | NOT PEER-REVIEWED | Posted: 19 November 2018 doi:10.20944/preprints201811.0459.v1

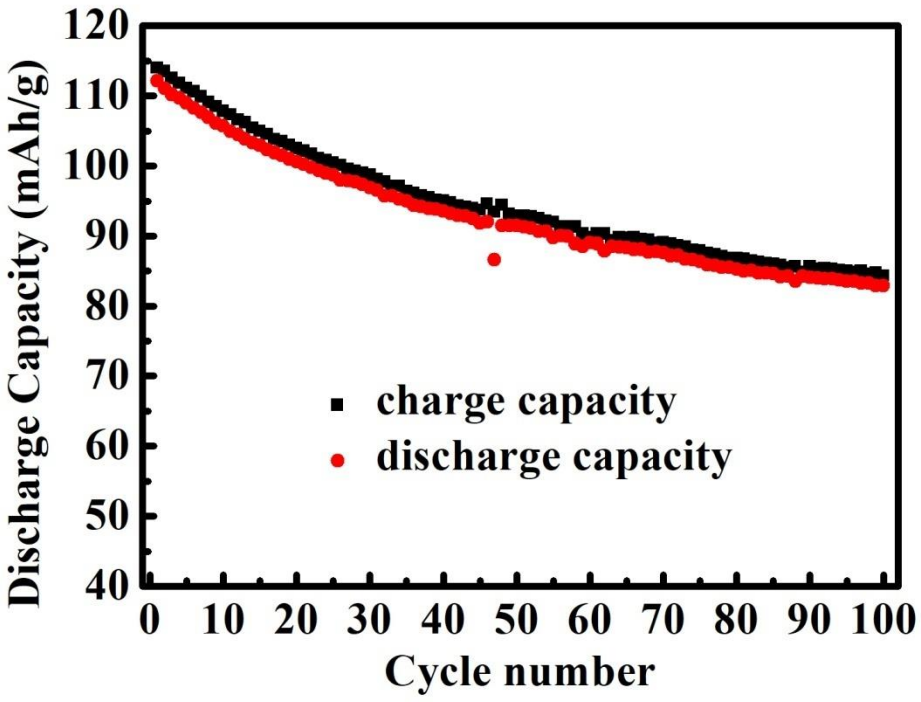

Fig.10 Cycle performance of $Li_{0.94}Na_{0.06}Mn_2O_4$ at a constant specific current of 740mA/g in the potential range of 3.0–4.3 V at 55℃.

Preprints (www.preprints.org) | NOT PEER-REVIEWED | Posted: 19 November 2018 doi:10.20944/preprints201811.0459.v1

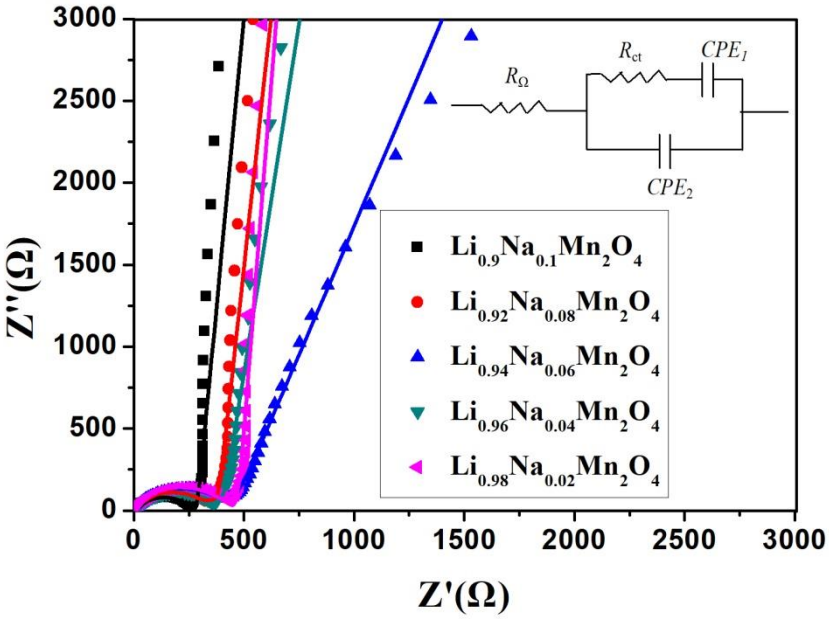

Fig.11 Electrochemical impedance spectra for $Li_{1-x}Na_xMn_{2-x}O_4$ (x=0-0.1).